Large-Scale Turbulence Characteristics of a Submerged Water Jet

R. S. ROSLER and S. G. BANKOFF

Northwestern University, Evanston, Illinois

Hot-wire anemometers, the chief tool in turbulence research, have had serious mechanical limitations for measurement in liquids. In 1955, a supported hot-film anemometer, based upon a previously known linear constant-temperature principle, was introduced by Ling and Hubbard (*1*) and subsequently improved by Ling (2, 3). The probe of this unit consisted of a 30 deg. glass wedge to which a 50 to 100 Å. thick platinum film was fused.

Despite these improvements, difficulties of probe stability, presumably due to electrolysis and/or scale formation, persisted in measurements of liquid turbulence. The problem of probe stability was overcome by the use of high purity distilled water throughout the system. Thereby extensive measurements could be made of mean velocity profiles, turbulence scales and intensities, and spectral energy distributions in a free water jet emerging into the bottom of an open tank.

Measurements also were made in a free air jet for comparison at the same exit Reynolds number (48,000). In contrast to most previous jet measurements, the jet exit profile obtained was not flat, but was that of fully developed turbulent pipe flow.

In air the root-mean-square velocity measurements with the hot-film unit were a factor of two to three low, possibly due to insufficient compensation for heat conducted into the glass backing. The bulk of the air data was therefore measured with a hot-wire anemometer. These problems of stability, compensation, and probe calibration were treated elsewhere (*20*)*.

The measurements divide naturally into those dealing with large- and small-scale turbulence characteristics of a free jet. In this work, the authors deal with the large-scale features such as mean velocity profiles, turbulent intensities, Reynolds stresses, and integral scales. Small-scale characteristics, such as microscales and spectral energy distributions, will be treated separately.

EXPERIMENTAL DATA

All the data for air and water were taken at a Reynolds number of 48,000. Hence the exit velocities at the center

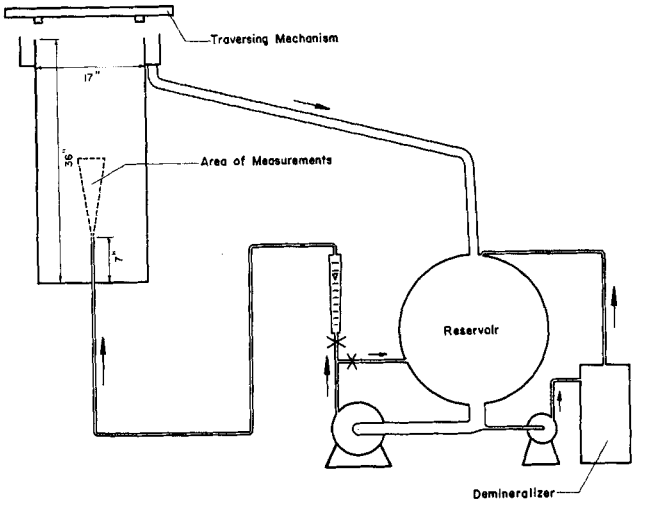

Fig. 1. Diagram of experimental apparatus.

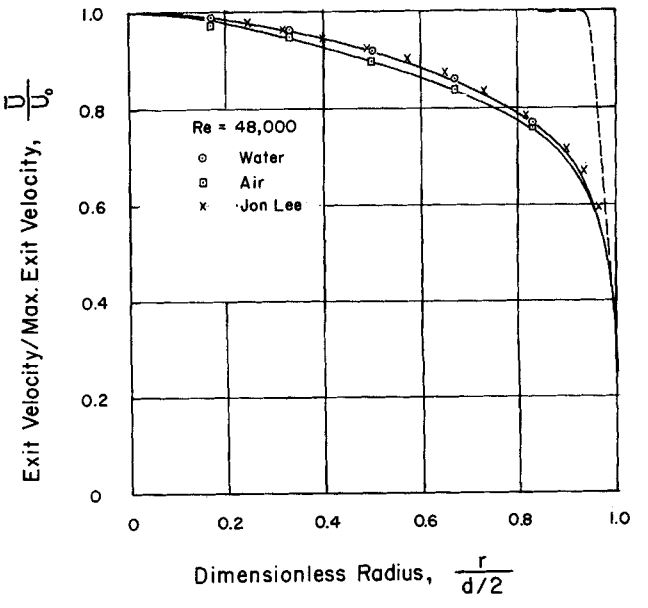

Fig. 2. Velocity distribution of issuing jet.

Mr. Rosler is with the United Technology Center, Sunnyvale, California.

* More recently, an analysis by W. G. Rose (*Am. Soc. Mech. Engrs.*, Paper No. 62-WA-11) of the corrections to the linearized response of a constant-temperature hot-wire anemometer to fluctuations in magnitude and direction of fluid velocity and in fluid temperature came to the attention of the authors. For the conditions in this work, the correction to the mean velocity is estimated to be of the order of 3% or less and to the turbulent intensity considerably less. This is less than the error in the determination of the mean readings of the meters.

TABLE 1.

	C	a/d	$\left(\frac{r_{1/2}}{x+a}\right)$	U_o (ft./sec)
Corrsin (9)	~5.3	−0.2	0.084	32.8
Corrsin (10)	6.55	−0.2	0.084	65-115
Hinze (11) published	6.39	+0.6	0.080	131
Hinze (11) corrected	5.9	−0.5	0.086	131
Polyakov (8)	6.54		0.086	
Taylor (12)	6.56	0	0.081	30-800
This work (air)	6.52	−0.8	0.086	259
This work (water)	6.58	−0.9	0.080	12.2

of the pipe (0.38 in. I.D.) were 259 and 12.2 ft./sec. for air (77.0°F. ± 0.1°F.), respectively. A diagrammatic sketch of the apparatus is shown in Figure 1.

Mean Velocities

The mean water velocity profile at the jet exit, shown in Figure 2, agrees with measurements taken by Lee in fully developed water pipe flow at a Reynolds number of 50,000 and is slightly flatter than the profile measured by Laufer (7) in air at the same Reynolds number.

Figure 3 shows a plot of the ratio of the maximum exit velocity to the axial mean velocity vs. diameters downstream. A straight line is drawn through the air and water data points so that the reciprocal of the slope (A) and the distance to the geometrical origin (a) may be evaluated for use in the relation

$$\frac{\overline{U_m}}{U_o}\frac{x+a}{d} = A \qquad (1)$$

The values of A are 5.26 and 5.39 for air and water, respectively, and about −0.8 and −0.9 for a/d.

Polyakov (8) investigated the dependence of jet propagation on the initial conditions. By assuming a constant angle of turbulent expansion and using the law of conservation of momentum, he showed that

$$A = C/F \qquad (2)$$

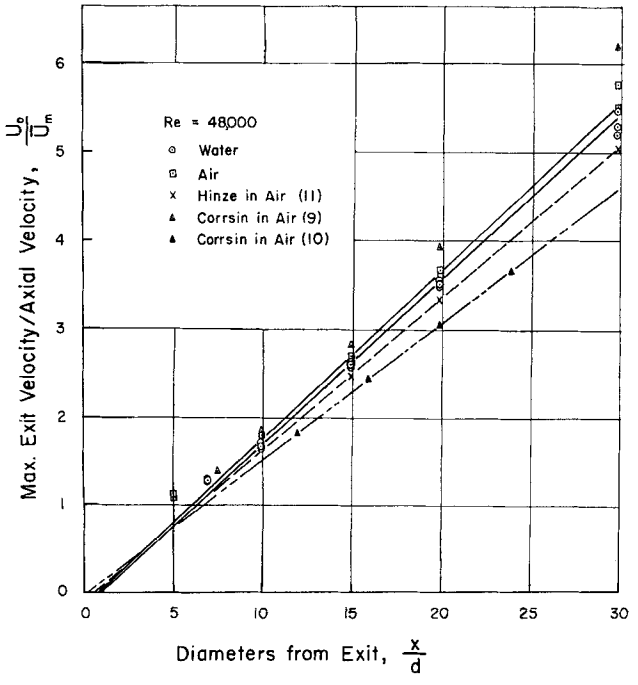

Fig. 3. Mean axial velocity on jet axis.

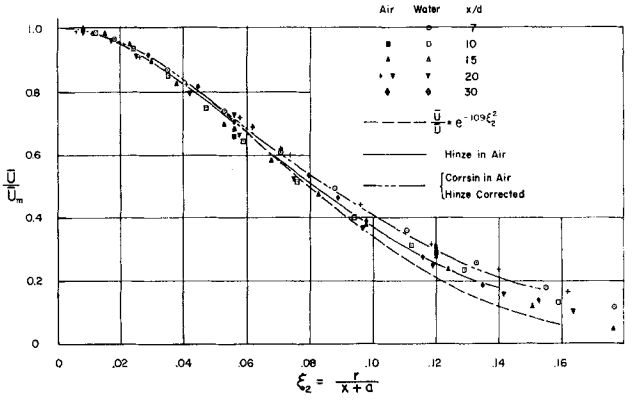

Fig. 4. Radial distribution of mean velocity.

where $C = 6.54$ as determined from his experiments in air (with flat and step-function initial profiles) and F, the form factor, is

$$F = \left[\int_o^1 \left(\frac{\overline{U_e}}{U_o}\right)^2 d\left(\frac{r}{d/2}\right)^2\right]^{-1/2} \qquad (3)$$

where $\overline{U_e}$ and U_o are the mean velocities at the jet exit at a radial distance r and at the center, respectively. The above is rearranged from Polyakov's original form (as is his constant, which was published as $7.38\sqrt{\pi/4}$).

From our exit profiles, F is 1.24 and 1.22 for air and water, respectively, and the values for the constant C are 6.52 and 6.58. This agrees with other published data, as shown in Table 1.

Velocity distributions in axially symmetrical free jets were measured by other investigators (13 to 17). However, in most cases, impact tubes were used with no apparent correction for the turbulent velocity fluctuations. Data taken in this way measure not mean velocities but momentum flux velocities. In a free jet with a turbulence level

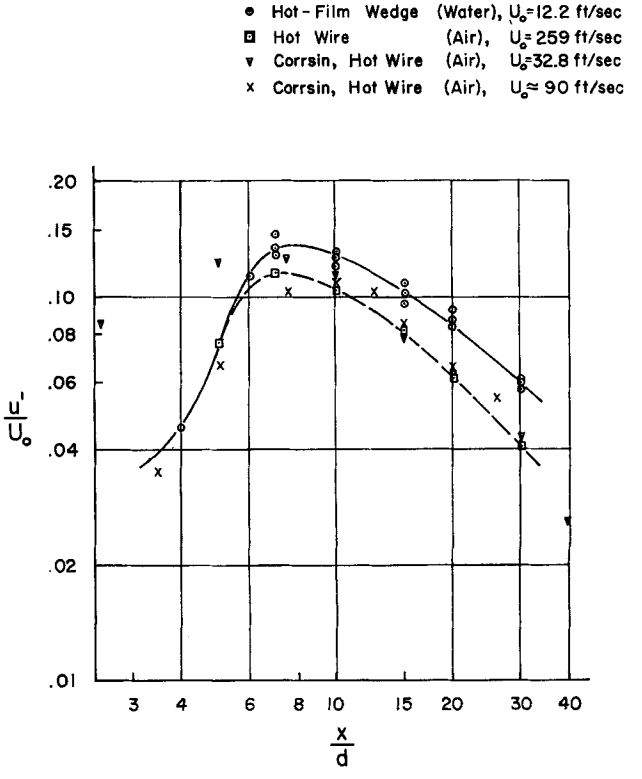

Fig. 5. Axial distribution of turbulent intensity.

of 50%, the momentum flux velocity is 12% greater than the mean velocity.

In addition to the authors' data of $U_o/\overline{U_m}$ vs. x/d for air and water, Figure 3 shows the data of Hinze and Corrsin. Corrsin's data of 1943 are high and do not lie along a straight line beyond 15 diam. His data of 1949 are in excellent agreement, however, as may be seen from the table.

Hinze and Van der Hegge Zijnen (*11*) appear to assume a positive value for a/d. This is not borne out by their data, replotted in Figure 3, which show a negative value for a/d. The serious implications of this discrepancy are seen in the plot of the mean profiles in Figure 4. The corrected plot deviates considerably from that shown in reference *11*. The corrected line is so close to Corrsin's data that both are shown by the same line. The dimensionless half-radius at which $\overline{U}/\overline{U_m} = 1/2$ is given in the third column of Table 1. Hinze and Taylor both used impact tubes but corrected for the effect of turbulence with the data of Corrsin. Implicit in this is the assumption that their turbulence level was the same as that of Corrsin.

The mean profiles for $\xi_2 < 0.12$ are described adequately by

$$\frac{\overline{U}}{\overline{U_m}} = e^{-C_1 \xi_2^2} \qquad (4)$$

where C_1 is 94 and 109 for air and water, respectively.

Root-Mean-Square Velocities

The axial distribution of turbulent intensity is shown in Figure 5 for air and water. The higher turbulent intensity of the water may be attributed to the motion induced by free surface waves.

In Figure 6 the root-mean-square velocity profiles are given with lines drawn through the water data points. The profiles beyond 10 diam. are similar for $\xi_2 > 0.10$. However, similarity of the profile over the whole cross section is achieved probably somewhere beyond 30 diam. The agreement with Corrsin's data is good. When allowances are made for the increase of turbulence level with free surface induced motion, mentioned previously, no noticeable effect (within the scatter of this type of measurement) of the kinematic viscosity on the turbulent intensity is found, as would be expected.

Reynolds Stress

When the mean velocity profiles are known, Reynolds stress $(\overline{uv})$ measurements may be checked independently by means of a momentum integral balance. With the momentum and continuity equations, discarding the small terms, and assuming similarity of profiles, one arrives at the following equation (*18*):

$$\frac{\overline{uv}}{\overline{U_m}^2} = \frac{\overline{U}}{\overline{U_m}} \frac{1}{\xi_2} \int_o^{\xi_2} \frac{\overline{U}}{\overline{U_m}} \xi_2 \, d\xi_2 \qquad (5)$$

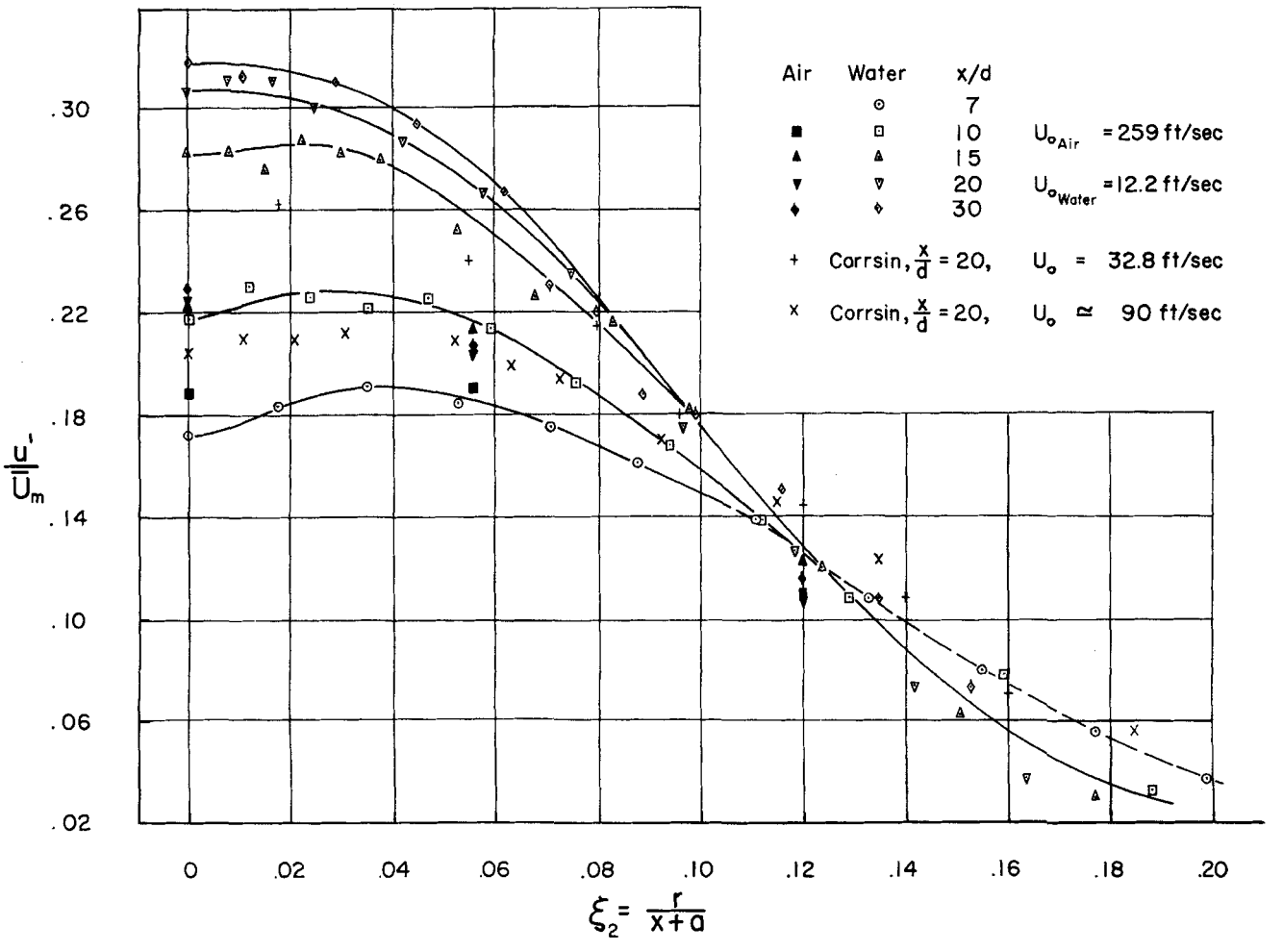

Fig. 6. Radial distribution of turbulent intensity.

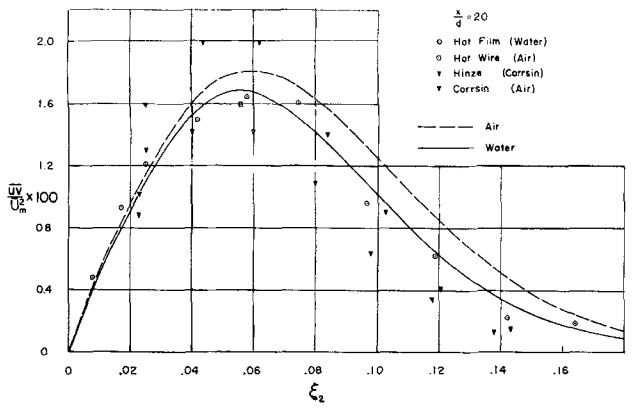

Fig. 7. Reynolds stress distribution at $x/d = 20$.

With Equation 4, this may be integrated:

$$\frac{\overline{uv}}{\overline{U_m}^2} = \frac{1}{2\,C_1\,\xi_2}\,e^{-C_1\xi_2^2}\,(1 - e^{-C_1\xi_2^2}) \qquad (6)$$

The curve for this equation, drawn for both air and water in Figure 7, agrees well with data at $x/d = 20$.*

Profiles of the Reynolds stress in water from 7 to 30 diam. downstream are shown in Figure 8 with the predicted water profile. At 7 and 10 diam. the Reynolds stress builds toward its equilibrium profile, which apparently is reached at 15 diam. The data at 15, 20, and 30 diam. agree well with the predicted profile.

Integral Scale

The macro or integral scale may be considered a measure of the average eddy size (*19*) and is related to the longest connection, or correlation distance, between the velocities at two points of a flow field. The integral scale (L) defined by Hinze (*18*) is

$$L = \frac{\pi}{2u'^2}\lim_{k\to 0} E_1(k) \qquad (7)$$

where k is the wave number and $E_1(k)$ is the turbulent energy in one wave number interval at k. Spectral measurements were made throughout the jet and will be presented elsewhere. The value of $E_1(0)$ was selected as the maximum value of $E_1(k)$. This also was done by Laurence (*5*) for his free jet measurements, which checked well with results from two-point measurements.

The good agreement, shown in Figure 9, of the ratio of integral scale in air to jet exit diameter with the data of Corrsin (*4*) and Laurence (*5*) in jets of different diameter (1.0 and 3.5 in.) indicates that the integral scale is directly proportional to the exit diameter and the exit profiles (both Corrsin's and Laurence's were flat) have negligible effect on the integral scale.

The large effect of the free surface on the integral scale, shown in Figure 9, may be attributed to the fact that the free surface induces relatively slow, large-amplitude movements.

THEORY

Based upon conservation of momentum, a momentum flux balance will be made for two reasons. First, it will provide a relationship between the constant (C) as obtained from the axial mean velocity distribution and the constant (C_1) used in the error function describing the radial mean velocity profile. Thereby, the consistency of the data will be checked. Second, it will show the effect of the turbulent intensity upon the mean velocity profile. The momentum flux balance is given when the flux at any cross section is equated to that at the jet exit:

$$\int_0^\infty (\overline{U^2} + \overline{P}/\rho)\,d(r^2) = \int_0^{(d/2)^2} (\overline{U_e^2} + \overline{P_e}/\rho)\,d(r^2) \qquad (8)$$

U and U_e are the instantaneous velocities in the jet and at the jet exit, respectively; and P and P_e are the corresponding pressure excesses over the pressure at infinity.

Hinze (*18*) shows this pressure difference term to be equal to the negative radial intensity, $-\overline{v^2}$. Hence

$$\int_0^\infty (\overline{U^2} + \overline{u^2} - \overline{v^2})\,d(r^2) = \int_0^{(d/2)^2} (\overline{U_e^2} + \overline{u_e^2} - \overline{v_e^2})\,d(r^2) \qquad (9)$$

Therefore

$$\overline{U_m}^2\,(x+a)^2 \int_0^\infty \left(\frac{\overline{U^2}}{\overline{U_m}^2} + \frac{\overline{u^2}}{\overline{U_m}^2} - \frac{\overline{v^2}}{\overline{U_m}^2}\right) d(\xi_2^2)$$

$$= U_o^2\,\frac{d^2}{4}\int_0^1 \left(\frac{\overline{U_e^2}}{U_o^2} + \frac{\overline{u_e^2}}{U_o^2} - \frac{\overline{v_e^2}}{U_o^2}\right) d\left(\frac{r}{d/2}\right)^2 \qquad (10)$$

where $\overline{U_m}$ is the maximum velocity at any cross section. Further

$$\frac{\overline{U_m}}{\overline{U_o}}\,\frac{x+a}{d} = (1/2F)$$

$$\left[\int_0^\infty \left(\frac{\overline{U^2}}{\overline{U_m}^2} + \frac{\overline{u^2}}{\overline{U_m}^2} - \frac{\overline{v^2}}{\overline{U_m}^2}\right) d(\xi_2^2)\right]^{-1/2} = C/F \qquad (11)$$

where

$$F = \left[\int_0^1 \left(\frac{\overline{U_e^2}}{U_o^2} + \frac{\overline{u_e^2}}{U_o^2} - \frac{\overline{v_e^2}}{U_o^2}\right) d\left(\frac{r}{d/2}\right)^2\right]^{-1/2} \qquad (12)$$

This definition of the form factor differs from the one given previously in Equation (3) in that the fluctuating components are included. In general, this contribution is negligible (less than 0.05% for the contribution due to pipe turbulence at the jet exit).

From Equation (11)

$$C = \frac{1}{2}\left[\int_0^\infty \left(\frac{\overline{U^2}}{\overline{U_m}^2} + \frac{\overline{u^2}}{\overline{U_m}^2} - \frac{\overline{v^2}}{\overline{U_m}^2}\right) d(\xi_2^2)\right]^{-1/2} \qquad (13)$$

This is essentially the equation given by Hinze and Van der Hegge Zijnen (*11*) except that they did not in-

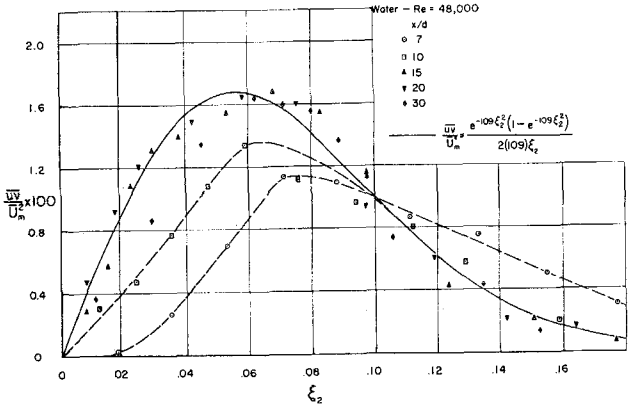

Fig. 8. Reynolds stress distributions at various axial positions.

* Corrsin's data, reproduced incorrectly by Hinze (*18*), are also shown. By private communication, Hinze points out that unpublished data by Van der Hegge Zijnen show measured values of Reynolds stress to be lower than theoretical values.

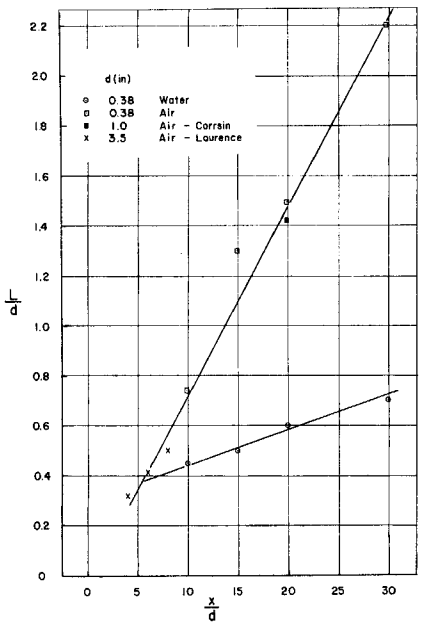

Fig. 9. Integral scale measurements along jet axis.

clude the $\overline{v^2}$ term which accounts for the pressure variation over a cross section of the jet. Since the authors did not measure $\overline{v^2}$, they estimated the value of $\int_0^\infty \frac{v^2}{\overline{U_m}^2} d(\xi_2^2)$ by determining the ratio of the radial to axial intensity integrated over the cross section. With Corrsin's data (9), this ratio was found to be 0.563. Hence, from the mean and root-mean-square profiles as measured at 20 diam.,

$$C_{\text{Air}} = \frac{1}{2}\left[(57.4 + 5.6 - 3.15)(10^{-4})\right]^{-1/2} = 6.46 \quad (14)$$

$$C_{\text{Water}} = \frac{1}{2}\left[(46.2 + 8.17 - 4.59)(10^{-4})\right]^{-1/2} = 7.09 \quad (15)$$

It is interesting to note the good agreement of C_{Air} as calculated from the axial (6.52) and the radial (6.46) profiles. The agreement of C_{Water} is not as good (6.58 and 7.09). However, the water data in Figure 3 could easily be represented by a line of smaller slope which would result in a value of C much closer to 7.09. Nevertheless, by introducing an extra mode of energy dissipation the free surface seems to have an effect on the water jet similar to that of a partial shroud.

A closer look at Equation (13), gives a better understanding of the effect of the turbulent intensity and also of the conditions necessary for C to be a true constant. It is a true constant only when both the mean and root-mean-square profiles are similar, and this implies that they are functions of ξ_2 only. For the mean velocity this occurs at about 10 diam., but for the root-mean-square velocity it occurs somewhere beyond 30 diam. However, for all practical purposes C is a constant beyond 10 diam. because the root-mean-square profiles make only a 4% to 8% contribution to C and do not change by a great percentage beyond 10 diam.

ACKNOWLEDGMENT

Financial support was provided by grants from the Research Corporation and the National Science Foundation. We also wish to thank both Dr. S. Corrsin and the referees for helpful comments.

NOTATION

a = distance to geometrical origin
A = reciprocal slope of axial mean velocity vs. diameters downstream
C = similarity constant, Equation (2)
C_1 = similarity constant, Equation (4)
d = jet exit diameter
$E_1(k)$ = one-dimensional turbulent energy spectrum function
F = form factor, Equation (3)
k = wave number
L = integral scale
P = excess pressure compared to conditions at infinity
r = radial distance
$r_{1/2}$ = jet velocity half-radius
u = axial velocity fluctuation
U = instantaneous axial velocity
$\overline{U_e}$ = mean velocity at jet exit at r
U_o = mean velocity at jet exit at center
v = radial velocity fluctuation
x = axial distance
ρ = density
ξ_2 = $r/(x + a)$

Subscripts

e = exit
m = maximum (center line)
o = exit center

Superscripts

— = time-average
= root mean square

LITERATURE CITED

1. Ling, S. C., and P. G. Hubbard, *J. Aerospace Sci.*, **23**, 890 (1956).
2. Ling, S. C., Ph.D. thesis, State Univ. of Iowa, Ames, Iowa (1955).
3. ———, *J. Basic Eng.*, **D82**, 629 (1960).
4. Corrsin, Stanley, and M. S. Uberoi, *Nat'l. Advisory Comm. Aeronaut. Tech. Note 2124* (1951).
5. Laurence, J. C., *ibid., 3561* (1955).
6. Lee, Jon H., Ph.D. thesis, The Ohio State Univ., Columbus, Ohio (1962).
7. Laufer, John, *Nat'l. Advisory Comm. Aeronaut. Tech. Rept. 1174* (1954).
8. Polyakov, E. I., *Soviet Phys.—Tech. Phys. (English Transl.)*, **5**, 1173 (1961).
9. Corrsin, Stanley, *Nat'l. Advisory Comm. Aeronaut.* WR *W-94* (1943).
10. ———, and M. S. Uberoi, *ibid., Tech. Note 1865* (1949).
11. Hinze, J. O., and B. G. Van der Hegge Zijnen, *Appl. Sci. Res.*, **A-1**, 435 (1949).
12. Taylor, J. F., E. W. Comings, and H. Grimmett, *Chem. Eng. Progr.*, **47**, 175 (1951).
13. Albertson, M. L., Y. B. Dai, R. A. Jenson, and Hunter Rouse, *Proc. Am. Soc. Civil Engrs.*, **74**, 1571 (1948).
14. Alexander, L. G., Thomas Baron, and E. W. Comings, *Univ. Illinois Bull.*, No. 413 (1953).
15. Cleeves, V., and L. M. K. Boelter, *Chem. Eng. Progr.*, **43**, 123 (1947).
16. Forstall, W., and E. W. Gaylord, *J. Appl. Mech.*, **12**, 241 (1962).
17. Miller, D. R., and E. W. Comings, *J. Fluid Mech.*, **3**, Part 1, 1 (1957).
18. Hinze, J. O., "Turbulence," pp. 41, 59, 384, 410, 432, McGraw-Hill, New York (1959).
19. Batchelor, G. K., "Theory of Homogeneous Turbulence," Cambridge University Press, Cambridge, England (1956).
20. Bankoff, S. G., and R. S. Rosler, *Rev. Sci. Instr.*, 33, 1209 (1962).

Manuscript received September 20, 1962; revision received March 29, 1963; paper accepted April 1, 1963.